Meteorol. Z. (Contrib. Atm. Sci.), Vol. 34 (2025), 35–55
Published online May 5, 2025

Open Access
Measurement Techniques

Eye2Sky – a network of all-sky imager and meteorological measurement stations for high resolution nowcasting of solar irradiance

Thomas Schmidt[1,*], Jonas Stührenberg[1], Niklas Blum[2], Jorge Lezaca[1], Annette Hammer[1], Stefan Wilbert[2], Bijan Nouri[2], Marion Schroedter-Homscheidt[1], Detlev Heinemann[1], Thomas Vogt[1]

[1] German Aerospace Center (DLR) – Institute of Networked Energy Systems, Carl-von-Ossietzky-Str. 15, 26129 Oldenburg, Germany
[2] German Aerospace Center (DLR) Institute of Solar Research, Calle Doctor Carracido N°44, Almeria, Spain
* Corresponding author: th.schmidt@dlr.de

With 11 figures and 6 tables

Abstract: The Eye2Sky network is a measurement network in north-western Germany consisting of 29 all-sky imagers (ASI) and 12 meteorological and solar irradiance measurement stations. Since 2018, the network collects high temporal and spatial resolution data for meteorological and especially solar energy related applications. Quality control schemes have been developed for the different sensors and are applied to the data in order to ensure a high quality. Quality controlled minute-resolution measurements (1 year) and ASI images (4 months) in the year 2022 are published for open access. Eye2Sky data is used in the development of new technologies and methodologies for accurate solar irradiance forecasts, facing the demand for grid integration of high shares of photovoltaic-generated power. The ASIs used in Eye2Sky record 180° field of view hemispherical sky images from fish-eye lensed cameras. Accompanied with local point measurements of solar irradiance components (global, direct and diffuse) a very short-term forecast of the solar resource is possible. A single ASI can provide such so-called nowcasts as minutely updated information. Nowcasts with a temporal resolution in the intra-minute range and a spatial resolution of a few meters are possible. Depending on the prevailing cloud dynamics the spatial coverage can be several kilometers and the maximum forecast horizon varies in the intra-hour range. The used ASI based approach shows superior forecasting results for the next minutes ahead compared to single ASI systems and traditional methods based on lower resolved satellite images or numerical weather prediction models. Eye2Sky, a unique network with multiple ASIs in a regional domain (about 110 km × 100 km coverage), enables an increased spatial coverage and an extended forecast horizon requested by many applications. In this article, the Eye2Sky network, its data and the quality control procedures are described. The potential of the network for solar energy applications and research topics is introduced.

Keywords: solar energy; solar irradiance; Eye2Sky; measurement network; All-Sky Imager; nowcasting

1 Introduction

The energy transition towards renewable energies leads to an increasing penetration of electric power grids with photovoltaic (PV) power generation. The volatility of solar irradiance in short-term periods is predominantly caused by changes in cloud cover. This volatility can be a critical issue for grid voltage and frequency and therefore the stability of the electrical grid (Notton et al. 2018). Additionally, regulatory limitations of allowed ramp-rates for PV plants are already effective or being discussed (Craciun et al. 2017).

Thus, accurate nowcasts of short-term PV power generation will support the integration of larger amounts of PV capacity (Antonanzas et al. 2016; Notton et al. 2018). For low voltage distribution grids, they potentially enable a higher PV penetration by utilizing short-term flexibility options and saving investments in the electrical grid (Mahdavi et al. 2017; Ghosh et al. 2017; Schmidt et al. 2017). For combined PV and battery systems nowcasts can support battery size optimization and management for ramp-rate regulations (Saleh et al. 2018; Ryu et al. 2021). Moreover, short-term updates of forecasted energy production in PV plants can

DOI: 10.1127/metz/2025/1245
Gebrüder Borntraeger Science Publishers, Stuttgart, www.borntraeger-cramer.com

assist energy traders by reducing deviations in predicted production and therefore saving money in intraday markets (Kaur et al. 2016).

The in-depth research on the spatial and temporal patterns of cloud induced solar irradiance variability leading to the aforementioned variability and uncertainty in PV power does help understanding the criticality of certain cloud conditions (Perez 2018). While many studies emphasized that temporal and spatial aggregation smoothes variability (e.g. Lave et al. (2012); Lohmann (2018); Ranalli et al. (2020)), high resolution data is needed to study small scale cloud structures, its dynamics and the effects of aggregation e.g. on the utility scale solar farm size, inside a distribution network with many distributed solar systems or inside local energy sharing communities.

For these data sets of solar resource variability on a scale of a few meters and minutes, high resolution local and up-to-date cloud cover information from all-sky imagers (ASI) are the fundamental information source.

ASIs provide high resolution images of the sky, recorded with cameras equipped with fisheye lenses providing a 180° hemispherical field of view. ASIs are able to resolve small-scale cloud cover and cloud fronts, responsible for short-term solar resource fluctuations. They can therefore improve the reduced spatial and temporal resolution of state-of-the-art solar forecasting methodologies such as numerical weather prediction models or satellite image-based forecasting. Due to the limited horizontal range of an ASI, the nowcast horizon and the spatial coverage for a single camera system is limited. In addition, both the spatial coverage of an ASI and the maximum forecast horizon are strongly dependent on the variable cloud height and dynamics as well as the position of the sun (azimuth and elevation), which determines cloud shadow projection. The cloud height determines the spatial coverage and together with cloud motion direction and speed the maximum forecast horizon at the location of interest will be limited. Typical nowcast horizons for systems with a single ASI range from a few minutes to 60 min ahead and cover a radius of 2 to 20 kilometres (Schmidt 2017; Nouri et al. 2022).

In recent years, several ASI-based nowcasting approaches have been developed. The objective to harness the high-level of detail in ASI data for the prediction of solar irradiance at a high spatial and temporal resolution makes accurate estimations of cloud properties the most important challenge. Several research activities have focused on the accurate determination of cloud properties from image information for enhanced solar radiation modelling (e.g. Fabel et al. 2022; Xie et al. 2020; Nouri et al. 2019a, b). In the past years, more and more machine-learning (ML) based approaches were upcoming (e.g. Paletta et al. 2021; Fabel et al. 2024). Knowledge and models from computer vision can obviously be helpful for the extraction of cloud properties such as segmentation tasks or cloud tracking. In most cases the models gain from large databases of training data collected at ASI sites. Based on deep learning, some studies used trained end-to-end models (e.g. Fabel et al. 2024; Meddahi et al. 2025) to predict the time series of solar irradiance based solely on a sequence of raw images taken at the site of interest. As these data-driven predictions are currently limited to point-based time series Meddahi et al. (2025) state, that future research should focus on developing spatially resolved forecasting methods, which leverage 2D irradiance maps or distributed sensor networks to predict variability across large-scale installations.

Nowcasting systems based on multiple ASIs have been studied experimentally to address the existing limitations of ASI-based systems, in particular regarding spatial coverage, forecast horizon and accuracy, as well as to represent the three-dimensional structure of clouds more adequately. Systems utilizing up to four ASIs have been studied e.g. by Nouri et al. (2018) and Peng et al. (2015). Systems based on larger ASI networks have been studied virtually (Mejia et al. 2018) and practically (Aides et al. 2020; Blum 2022; Blum et al. 2022; Chu et al. 2022). Further ASI networks are operational[1] or have been planned[2]. Beyond such ASI networks for day-time cloud observations, further meteorological networks have been operated in various contexts. E.g. Lorenz et al. (2022) introduced a regional network of 40 measurement stations of global irradiance distributed over an area of around 200 km × 200 km dedicated to real-time upscaling of PV production. In the HOPE experiment (Macke et al. 2017), 99 photodiode pyranometers measured global irradiance in an area of 10 km × 12 km. Simultaneously 6 ASIs observed the sky in the same area. (Schmidt et al. 2016) evaluated nowcasting performances at the pyranometer network based on one of the ASIs. In addition, but outside the context of solar irradiance nowcasting, a number of astronomical ASI networks have been operated for night-time imaging dedicated e.g. to the detection of fireballs (Spurny 1997; Howie et al. 2017).

Eye2Sky is an operational research network of ASIs installed and operated by DLR in northwest Germany. At 29 different locations, all-sky imagers record images every 30 seconds. At 12 locations, the images are complemented by solar irradiance and meteorological measurements. The Eye2Sky network covers about 110 km × 100 km with a focus at the city of Oldenburg. It has a lower station density in rural areas and a higher density in the city of Oldenburg. The network is under ongoing development since 2018 and already provides more than five years of sky images and high-quality measurements.

1 National Solar Repository of Singapore (NSR) https://www.solar-repository.sg/sky-cameras

2 https://www.trouw.nl/duurzaamheid-economie/pleidooi-wolkencamera-s-kunnen-piek-en-dip-in-stroomvoorziening-voorkomen~b5486ffa/

Compared to existing other measurement networks and data sets, Eye2Sky comes with a unique density of ASI data (see Nie et al. (2024) for a list of existing open-source ASI data sets). In the city of Oldenburg, 13 ASIs allow an almost full coverage of the city (about 12 km × 15 km) and an extension of the forecast horizon of more than 30 min in 50% of the time (Schmidt et al. 2023a) using the well-tested ASI-nowcasting model described in Blum et al. (2022, 2021) and Logothetis et al. (2022). Fig. 1 shows an example of global horizontal irradiance (GHI) nowcasting using 17 ASIs for the city of Oldenburg. Next to forecast horizon and coverage, the effect of overlaps in camera data and redundancy on the nowcast results can be studied. Moreover, together with ground based solar irradiance measurements high resolution and accurate solar irradiance analysis maps providing information with 30 seconds of temporal and up to 50 meters of spatial resolution are generated. This analysis data is a unique basis for the validation of spatial and temporal patterns in other coarser resolution data sets (e.g. satellite-derived data or numerical weather prediction models).

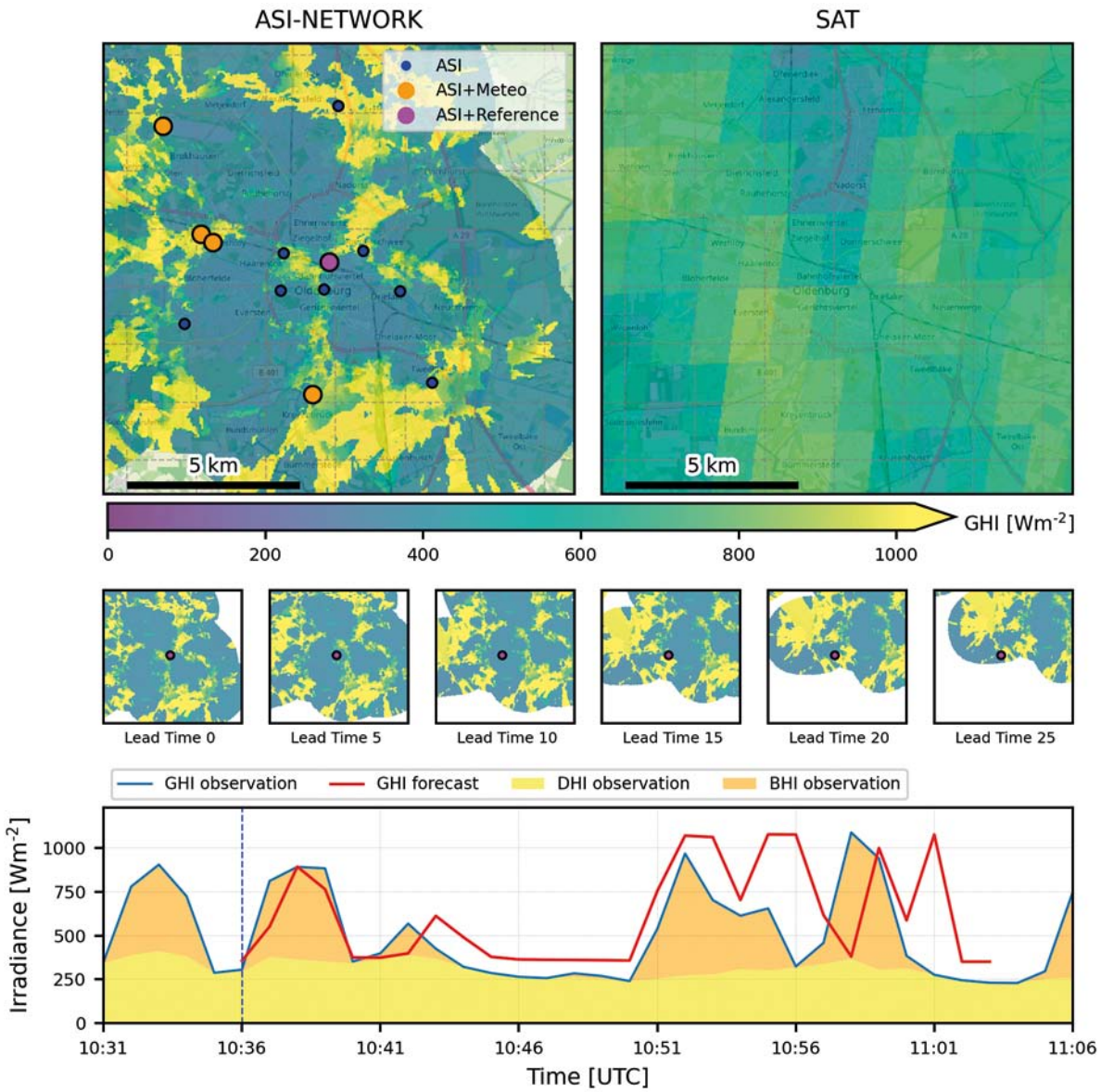

Fig. 1. Example of a nowcast of global horizontal irradiance (GHI) for the city of Oldenburg with ASI images of 17 stations included in the modelling for 2022-06-26. For comparison of the level of detail, GHI derived from a MSG satellite image (Observation time 10:41 UTC) is shown (top right). In this scenery, small-scale clouds from south-western direction were approaching the city. The predicted GHI maps (center row) and timeseries (bottom, red line) for the location in the center of the map (magenta circle) shows good agreement with observations highlighting the cloud induced short-term variability in solar radiation. DHI (diffuse horizontal irradiance) and BHI (direct horizontal irradiance) are the observed radiation components.

Moreover, this data set allows to study high-resolution spatio-temporal solar variability and aggregation effects (Blum et al. 2022; Schmidt et al. 2023b). This could be crucial for the integration of large amounts of PV into electrical grids.

Nowcasting of solar irradiance with Eye2Sky data is based on the analyzed solar irradiance distribution along with cloud dynamics. Depending on the cloud dynamics present, a short term forecast of the solar irradiance distribution in minutely resolution using all ASIs in the network can be computed for the next minutes up to 2 hours.

In addition, a multiple data source approach using on-site irradiance measurements and satellite-based irradiance nowcasts together with ASI based nowcasts contributes to further improvements in accuracy, nowcast horizon and spatial coverage.

In the following, we present our measurement network in Section 2 and the instrumentation of the different stations in Section 3. We describe the data sets in Section 4 and the quality assessment of solar irradiance and auxiliary measurements in Section 5. The potential of the nowcasts derived with our network is summarized for different applications Section 6. The published data set is described in Section 7.

2 Network

The Eye2Sky network has been initiated with the first installations in 2018 and has been growing until today. In January 2024 in total 29 measurement stations in the city of Oldenburg and the surrounding area were active (Fig. 2). The network domain is a rather flat area with a marine climate due to presence of the north sea.

At the stations the same ASI camera type in order to standardize ASI operations in such a network are operated. This helps to gain experience in standardization of the station deployment in larger scale networks.

Additionally, 8 ceilometers (two operated by DLR, six operated by German Weather Service DWD) supplement the network with cloud height reference data. Table 1 summarizes all stations operated by DLR. The instrumentation of the stations can be grouped in three different types. Every location is equipped with an ASI. Twelve stations provide meteorological and irradiance measurements. Two of them are reference stations (REF) using a solar tracker with ISO 9060 spectrally flat class A radiometers used for validation and providing additional measurements. Ten stations

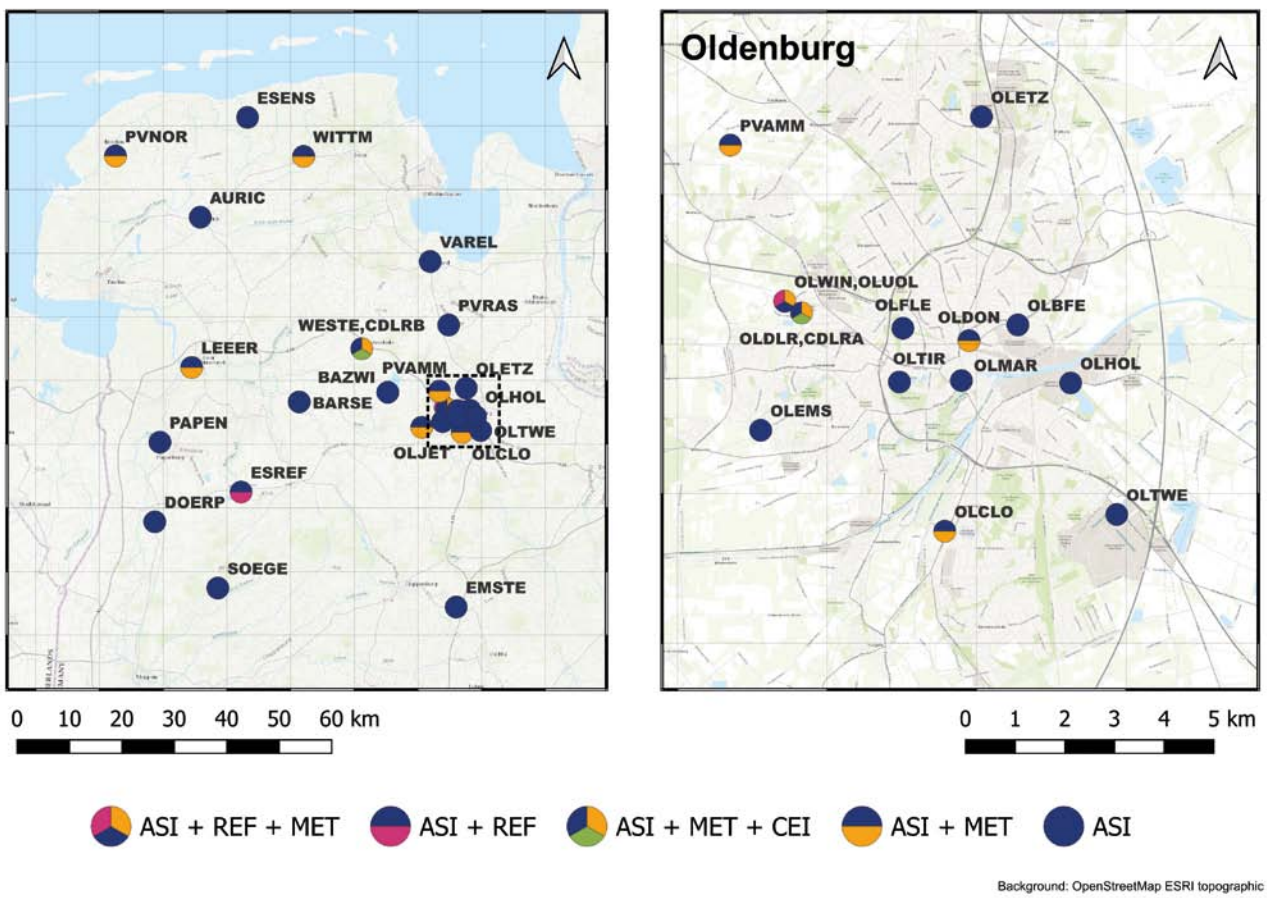

Fig. 2. Distribution of Eye2Sky stations active in summer 2023. Two meteorological stations (REF) are equipped with high quality solar trackers and additional meteorological instruments. MET stations provide solar radiation measurements based on rotating shadowband irradiometers. Stations marked with CEI are equipped with ceilometers.

include a rotating shadowband irradiometer (RSI) (station type "MET"). The most important measurement station is the reference station OLWIN, located in the north-west of Oldenburg at the university campus Wechloy and main building of DLR's Institute of Networked Energy Systems. Regular maintenance and cleaning, additional long-term and experimental instrumentation and a calibration stand for RSI pyranometer units allow for high quality measurements. Redundancy with RSI-based OLUOL station allows for site-by-site comparisons (See chapter 5 for more details on data quality). The nearby OLDLR station provides a second ASI for short-distance stereography. Additionally, an on-site ceilometer provides valuable cloud height information.

The locations for the measurement stations have been chosen based on a preselected distribution and the compliance with suitable properties. The distribution was selected to fulfill the following requirements:

- Fair coverage of the low-voltage electricity distribution grid of the local distribution system operator (DSO) *EWE Netz* between Oldenburg in the east, the Dutch border in the west and the North Sea coast in the north

Table 1. Table of all active stations in the Eye2Sky network giving its ID, domain, station type, geographical coordinates, altitude of instrumentation above sea level, height above surface and its installation date. The station type REF refers to a solar tracker station. All MET stations except of PVAMM include RSI-based solar irradiance measurements and an all-sky imager. ASI indicates camera-only stations and CEI provides ceilometer measurements.

#	Station ID	Place	Domain	Type	Latitude [°N]	Longitude [°E]	Altitude (MASL)	Height above ground [m]	Installation date
1	OLWIN, OLUOL	Oldenburg	Suburban	REF, MET	53.15348	8.16192	21	15	25 June 2019
2	OLDLR, CDLRA	Oldenburg	Urban	MET, CEI	53.15137	8.16701	21	9	3 April 2018
3	OLCLO	Oldenburg	Urban	MET	53.11200	8.21004	22	14	9 Nov. 2018
4	OLDON	Oldenburg	Urban	MET	53.14637	8.21733	28	20	26 Sept. 2018
5	PVAMM	Metjendorf	Urban	MET	53.18160	8.14560	11	2	15 Okt. 2019
6	OLTWE	Oldenburg	Urban	ASI	53.11502	8.26172	16	7	14 Sept. 2021
7	OLEMS	Oldenburg	Urban	ASI	53.13021	8.15472	20	12	10 Dez. 2019
8	OLBFE	Oldenburg	Urban	ASI	53.14921	8.23201	22	14	3 Febr. 2020
9	OLETZ	Oldenburg	Urban	ASI	53.18670	8.22108	25	4	16 Sept. 2020
10	OLMAR	Oldenburg	Urban	ASI	53.13918	8.21504	30	16	9 Nov. 2018
11	OLHOL	Oldenburg	Suburban	ASI	53.13873	8.24786	16	10	17 Dez. 2018
12	OLFLE	Oldenburg	Urban	ASI	53.14861	8.19747	23	15	26 Nov. 2018
13	OLTIR	Oldenburg	Urban	ASI	53.13892	8.19640	39	30	26 Okt. 2018
14	ESREF	Esterwegen	Rural	REF, ASI	53.01063	7.58575	8	2	3 April 2019
15	WITTM	Wittmund	Suburban	MET	53.57694	7.76241	8	5	10 Feb. 2022
16	WESTE, CDLRB	Westerstede	Suburban	MET, CEI	53.25335	7.92658	19	10	2 Dez. 2020
17	LEEER	Leer	Rural	MET	53.22173	7.44668	17	12	21 Aug. 2019
18	PVNOR	Norden	Rural	MET	53.57749	7.23156	2	2	11 July 2019
19	OLJET	Friedrichsfehn	Suburban	MET	53.12040	8.09583	17	4	10 July 2019
20	BAZWI	Bad Zwischenahn	Rural	ASI	53.17959	7.99990	20	10	11 Sept. 2020
21	PAPEN	Papenburg	Rural	ASI	53.09513	7.35701	87	77	16 Nov. 2021
22	EMSTE	Emstek	Rural	ASI	52.81489	8.19291	74	20	16 Jan. 2020
23	PVRAS	Rastede	Rural	ASI	53.29334	8.17172	19	3	12 Mar. 2021
24	BARSE	BarSSel	Rural	ASI	53.16337	7.75002	10	6	25 Okt. 2019
25	ESENS	Esens	Rural	ASI	53.64210	7.60411	12	5	2 Aug. 2019
26	SOEGE	Soegel	Suburban	ASI	52.84727	7.52025	55	10	4 Nov. 2019
27	DOERP	Doerpen	Rural	ASI	52.96002	7.34255	15	6	10 Dez. 2019
28	VAREL	Varel	Suburban	ASI	53.40032	8.11957	10	5	2 Aug. 2019
29	AURIC	Aurich	Rural	ASI	53.47473	7.47082	11	5	9 Dez. 2019

Fig. 3. Photos of two Eye2Sky stations. (a) Meteorological station OLCLO in southwest of Oldenburg mounted on the flat roof of an office building. (b) Instrumentation of station PVNOR installed in a solar plant showing the ASI (left), the RSI (center) and the tilted pyranometer and PAR sensor (right).

- High density of stations in the city of Oldenburg for a good coverage of the urban area with many overlapping camera images
- A fair distribution of meteorological measurements for calibration and validation of solar irradiance analysis and forecasts
- Ceilometers measuring cloud base height are placed in Oldenburg (at the reference site) and Westerstede ≈20 km north west from Oldenburg (opposite of main direction of cloud motion). Both instruments are supplemented by ceilometers operated by German National Weather service (DWD) located in Friesoythe, Emden, Lingen, Bremerhaven, Diepholz and Norderney (https://e-profile.eu) which provide additional cloud height information.

Furthermore, suitable locations must offer secure access for maintenance, protection against theft and vandalism, electrical power supply, a sufficient mobile network reception, as well as free field of view with a minimum of obstacles in the surroundings. Table 1 summarizes the basic properties of all Eye2Sky stations.

Except for the two reference stations, all stations are mounted on poles. The poles have been mounted depending on the surface type with a stand for flat roofs or brackets for wall mounting (see Fig. 3a).

The surface type varies between locations which is why standards of the World Meteorological Organization (WMO) for the measurement of air temperature and relative humidity cannot be followed. Moreover, the measurement height

above ground does also not fulfill the WMO requirement of an installation height of 2 m above ground. Both measurements therefore are probably biased, but reflect ambient conditions on roof tops as relevant for many PV installations.

3 Instrumentation

The all-sky imagers (ASIs) of Eye2Sky are surveillance cameras of type Mobotix Q25 6MP color version with a fisheye lens providing 180° field of view. All cameras are equipped with an additional ventilation and heating unit protecting the lens from dust, dew, snow and ice. An automatic cleaning system based on spray nozzles pointing at the lens is currently under testing. Moreover, camera's software integrated event detection is currently tested to automatically detect images disturbed by birds, insects or even human faces.

The cameras are calibrated geometrically describing lens distortion (internal calibration) and external orientation after installation. The internal calibration is performed using a method developed by Scaramuzza et al. (2006). The external orientation, i.e. the azimuth deviation from geographical north, is calculated during full moon nights detecting the moon's position relative to the camera's orientation as described by Blum (2022). All cameras are set up with the same configuration files to allow further processing without adaptation for single cameras. All ASIs are set to a constant exposure time of 160 µs and a constant color temperature of

Table 2. Table of stations with solar irradiance and meteorological measurements. * The GTI sensor at PVAMM is orientated to 187° according to the orientation of the PV plant. ** At station OLJET the RSI motor has been switched off and hence only GHI measurements are available here. ***At station PVAMM a combined sensor Lufft WS 600 is installed at 2.3 meters above ground.

	Type	ASI	GHI	DHI	DNI	GTI	Temp	rel Humidity	Pressure	Rain	Wind speed	Wind direction
OLWIN	Tracker station		EKO MS-80	EKO MS-80	EKO MS-56		CS215	CS215		Thies Clima Rain Gauge		
ESREF	Tracker Station	Mobotix Q25	K&Z CMP-21	K&Z CMP-21	K&Z CMP-21	Li-Cor 200 30° / 180°	CS215	CS215	Vaisala PTB110		Th. Friedr. 4310 Ultrasonic 10m	Th. Friedr. 4310 Ultrasonic 10m
PVAMM	PV plant monitoring	Mobotix Q25	EKO MS-80			EKO-MS80 30°/187° *	Lufft WS600	Lufft WS600	Lufft WS600	Lufft WS600	Lufft WS600 ***	Lufft WS600 ***
OLUOL	RSI Station	Mobotix Q25	CSPS Twin-RSI	CSPS Twin-RSI	CSPS Twin-RSI	Li-Cor 200 30°/180°	CS215	CS215				
OLDLR	RSI Station	Mobotix Q25	CSPS Twin-RSI	CSPS Twin-RSI	CSPS Twin-RSI	Li-Cor 200 30°/180°	CS215	CS215				
OLCLO	RSI Station	Mobotix Q25	CSPS Twin-RSI	CSPS Twin-RSI	CSPS Twin-RSI	Li-Cor 200 30°/180°	CS215	CS215				
OLDON	RSI Station	Mobotix Q25	CSPS Twin-RSI	CSPS Twin-RSI	CSPS Twin-RSI	Li-Cor 200 30°/180°	CS215	CS215				
WESTE	RSI Station	Mobotix Q25	CSPS Twin-RSI	CSPS Twin-RSI	CSPS Twin-RSI	Li-Cor 200 30°/180°	CS215	CS215				
WITTM	RSI Station	Mobotix Q25	CSPS Twin-RSI	CSPS Twin-RSI	CSPS Twin-RSI	Li-Cor 200 30°/180°	CS215	CS215				
LEEER	RSI Station	Mobotix Q25	CSPS Twin-RSI	CSPS Twin-RSI	CSPS Twin-RSI	Li-Cor 200 30°/180°	CS215	CS215				
PVNOR	RSI Station	Mobotix Q25	CSPS Twin-RSI	CSPS Twin-RSI	CSPS Twin-RSI	Li-Cor 200 30°/180°	CS215	CS215				
OLJET	RSI Station	Mobotix Q25	CSPS Twin-RSI	**	**	Li-Cor 200 30°/180°	CS215	CS215				

5500 K. Due to technical reasons the actual exposure time of daytime images becomes 149 µs. Moreover, each ASI image is cropped to a rectangle with a size of 2048 pixel × 2112 pixel.

The meteorological stations have additional rotating shadowband irradiometers (RSI) and provide direct normal (DNI), diffuse horizontal (DHI) and global horizontal (GHI) irradiance (Fig. 3b). The RSIs are CSP Services TwinRSIs (Geuder et al. 2012). Tilted pyranometers (LiCor200) and photosynthetically active radiation (PAR) sensors (LiCor190) at 30° tilt angle pointing south (180° azimuth angle) measure global tilted irradiance (GTI) and tilted PAR. PAR measurements can be used among others in the context of agrivoltaic allowing the dual use of land for both agricultural activities and solar power conversion (Ma Lu et al. 2022). Ambient air temperature and relative humidity as needed for PV power modelling is measured with a combined sensor (Campbell Scientific CS215).

The reference stations provide irradiance data measured with a solar tracker and thermopile radiometers along with additional meteorological measurements (wind, precipitation, barometric pressure). Table 2 summarizes the instrumentation used at MET and REF stations.

The meteorological data acquisition is performed by high-quality data loggers (Campbell Scientific CR1000X / CR6 at OLWIN station) pushing data in real time to a central server. Real-time ASI images are pulled from the central server which secures the synchronized acquisition of images. Ceilometer data is pulled from each device. The real time data transfer is secured via 4G mobile network routers establishing a connection to a WireGuard VPN. High signal strengths allow the transfer of camera images (≈100–400 kB) in a few seconds. Nevertheless, delays occur when signal strength is low. Clock synchronization is also performed in between the central server and the devices (data loggers, ceilometer). Ceilometers of type Lufft CHM 15k are used with a measurement interval of 15 seconds.

4 Data set

4.1 Database

The data base consists of ASI images, in-situ meteorological and cloud height measurements since 2019. Raw ASI images (jpg-format) are stored every full 30 s during daytime and minutely in full-moon nights (>70 % moon-phase) for calibration purposes. Fig. 4 shows an example of 29 synchronized ASI images. Meteorological measurements are sampled every second. Raw logger data (csv-format) is stored in the database. After a post-processing including an automatic quality control (see chapter 5) 1 min averaged and flagged data are stored in a compressed HDF5 file format for further usage. Cloud height data from the six aforementioned ceilometers are stored as raw data in daily netcdf files. All timestamps of Eye2Sky data are given in UTC.

Data gaps due to a number of reasons are inevitable. In particular the availability of data from the network is reduced due to different installation dates of single stations, failures of complete stations (due to power loss or connection loss), failures of single instruments, flagging and removal of data due to quality issues. Nevertheless, Eye2Sky achieves an availability of 99.5 % of ASI images in summer 2022. A full overview is provided in Fig. 5a and 5b.

4.2 ASI images

ASI images are stored in jpg-format. Details of the image format are given in Table 3. Each ASI data set is accompanied with meta data including mask files for excluding parts of the image and calibration information for the internal and external orientation of the camera.

Mask files are used to mask out non-sky and static objects for further processing. These mask files are automatically generated based on daily average images. Averaging images will smooth out dynamic changes in the sky part mainly due to cloud motion and therefore sharpen edges along static objects. This allows an automatic edge detection algorithm to detect the outline of the sky-only part. New mask files are generated when the camera's horizon changes. This can happen after a new camera has been set up, after realignment of the camera, or if new objects such as buildings, trees or antennas appear in the field of view of the camera. The mask files do not mask out non-static objects such as birds, insects or persons in the field of view. The filename corresponds to the date since when the mask is valid. Fig. 6 shows an example of applied mask files and external orientation for the station OLMAR, which shows the biggest obstacles (nearby church) in the field of view of all ASIs.

The calibration of the internal orientation is hardware-dependent and performed with the OmniCalibToolbox (Scaramuzza et al. (2006)) in a laboratory before installation. Parameters are defined according to the software for the real image center coordinates and lens distortion.

The external calibration provide parameters for the orientation of the camera after mounting. It consists of pitch, yaw and roll angles of the rotation around the three perpendicular axes. They are used to identify the camera's orientation to north and its tilt due to a non-horizontal alignment. The calibration is performed automatically after each full moon period according to the theoretical and the real moon position in the image. The moon is preferable to the sun for calibration, as its contours and therefore its position are better detected. Images from nights in which a moon phase of more than 70 % is present are used to record a sufficient amount of images with a clearly visible moon. The filename of the external calibration corresponds to the night of full moon.

4.3 Meteorological data

Meteorological data is provided as 1 min averaged raw and quality-controlled values. Data is stored internally in daily HDF5 files for each measurement station. For public usage,

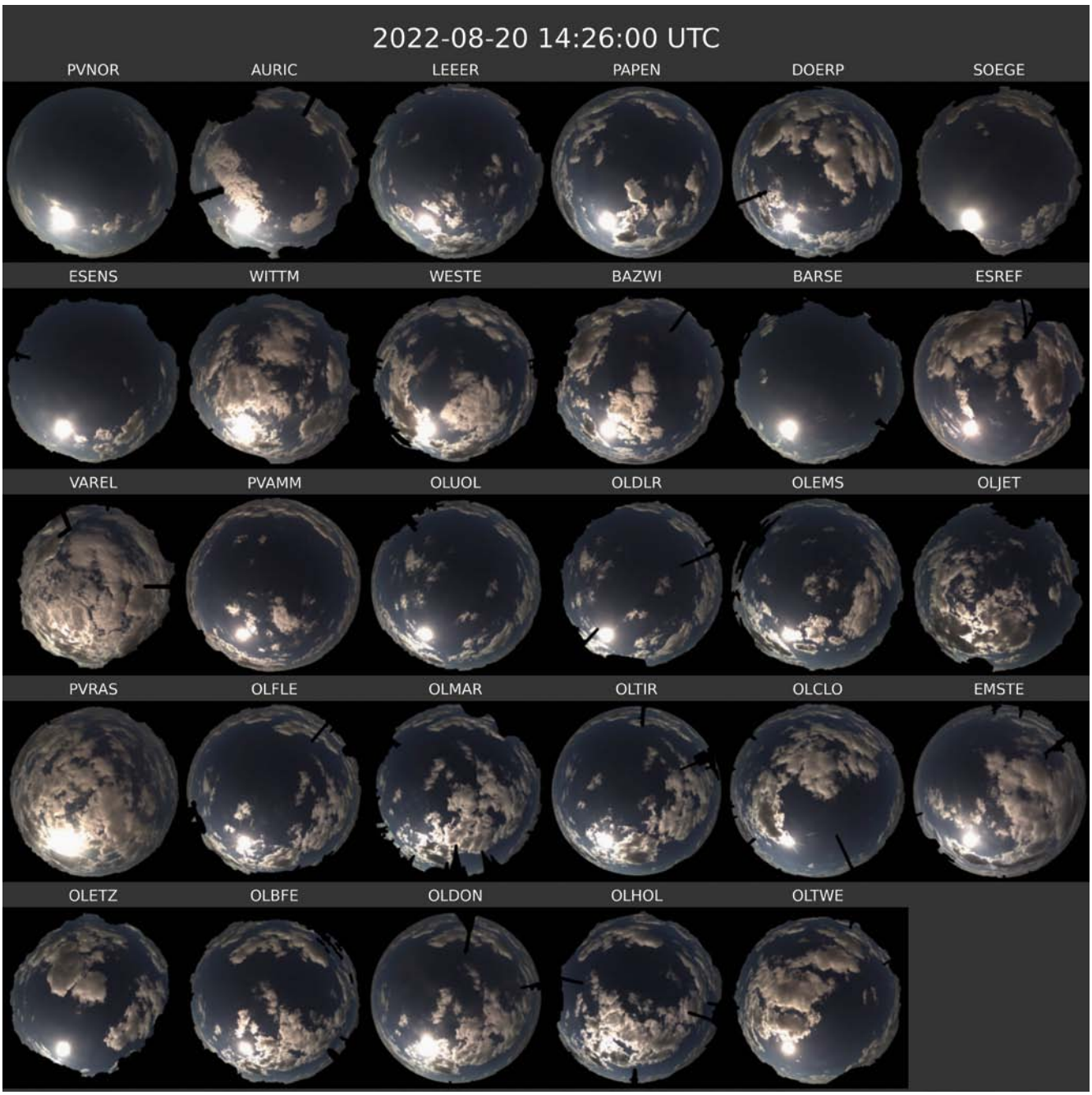

Fig. 4. Example collage of 29 camera images taken at 14:26 UTC on 20 August 2022. The collage shows images with masked horizon.

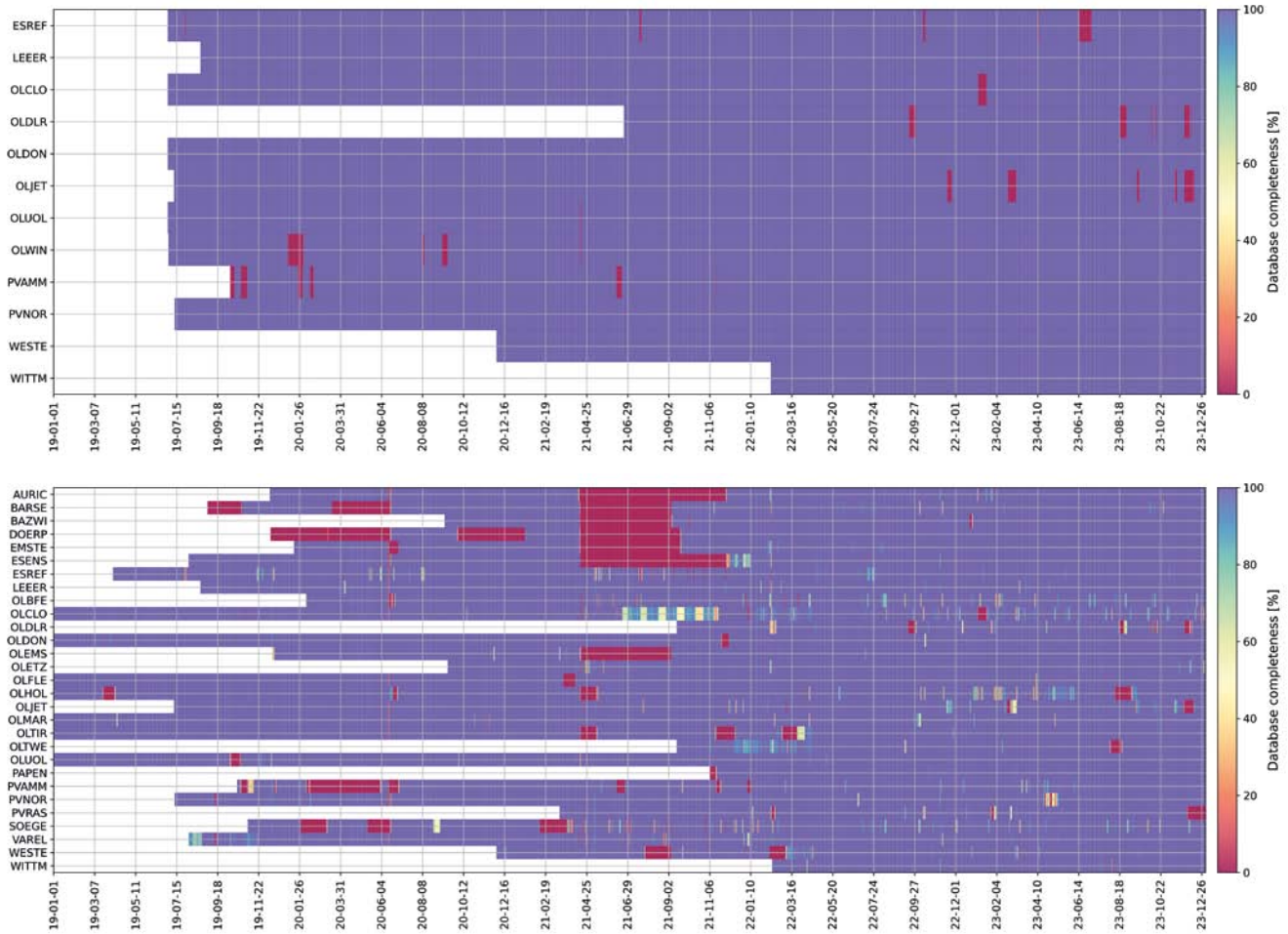

Fig. 5. Database completeness for ASI images (a) and meteorological data (b). Installation date, short-, mid- and longterm data gaps can be recognized quickly. (a) ASI images database until end of 2023. (b) Meteorological file database until end of 2023. This figure only shows missing daily files indicating a complete disconnection or station failure.

Table 3. Description of ASI images: YYYYMMDD_HHMMSS corresponds to the timestamp when the image has been captured in UTC. **EXP** corresponds to the timestamp (in UTC) when the image has been captured. During daytime an exposure time of 160 µs is set. During nighttime the exposure time is 80000 µs.

Data set	Description and Size
Hemispheric image	
Sampling rate	30 s
Image size	2112 pixel × 2048 pixel
File size	≈100–400 kB per image
File type	JPG
Filename	YYYYMMDD_HHMMSS_EXP. jpg
Remarks	night-time images only during full moon

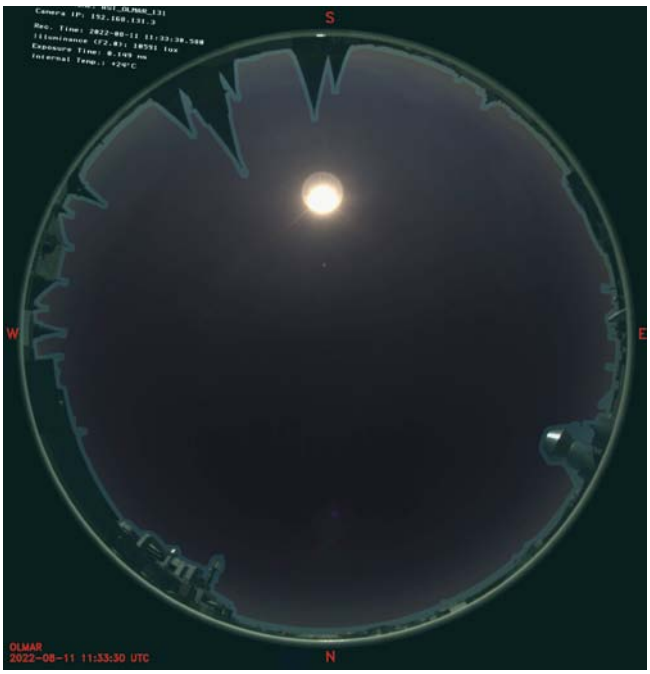

Fig. 6. Example ASI image of station OLMAR in the city center of Oldenburg taken at 11:33:30 UTC 11 August 2022. In this image, the mask file has been applied (transparent overlay) and the image has been rotated to the true North-South axis according to the external orientation parameters. The amount of rotation is visible at the rotated image caption in the top-left of the image.

data is exported from the internal database in the more common netcdf file format. The file structure and meta data follow conventions from the scientific community for easier handling (see https://libinsitu.readthedocs.io).

5 Quality control (QC)

Generally, high availability and data quality is guaranteed by using high quality instrumentation, robust data connection, regular data quality checks and maintenance visits. Because the stations in the network do not have their local on-site maintenance team available, they can only be cleaned in longer time intervals. It is preferable to visit only those stations having a need of cleaning. Therefore, a specific quality assurance procedure was decided upon.

For Eye2Sky, one measurement station is used as reference. There, the high data quality is achieved by using tracker-based solar irradiance measurements along with weekly cleaning of its thermopile radiation sensors and ASI. Other stations are visited less often for cleaning and maintenance. Maintenance visits include cleaning of sensors, control of electrical connections and the alignment of sensors. Sensor replacement is done in case of failures or after the calibration interval. Internal logbook entries and photos are used for documentation.

For the stations with no regular maintenance, failures and quality issues are monitored by regular automatic and manual data control and station-by-station comparisons of daily means. In such a dense network station-by-station comparisons with a high-quality and well-maintained reference station may result in a close-to-equal data quality even for less maintained stations. Especially for daily averages correlations are expected to be high for nearby stations and reduced with distance to the reference station (see Fig. 9 and Fig. 2 for the map of stations). Based on station pair statistics, one can derive thresholds for daily mean differences indicating erroneous measurements (e.g. soiling, dew or ice). This idea is used for meteorological time series data as well as for images from ASI. So far, station-by-station comparisons are performed visually to get a first impression of the quality of Eye2Sky station data and for scheduling of maintenance. Appropriate metrics and thresholds are currently investigated. Therefore automatic procedures have not been implemented yet, as it requires several years of data to set thresholds properly. This data collection period is still ongoing.

The following subsections describe the details of the data quality control.

5.1 Quality control for ASI

Data quality of ASI images is affected mainly by soiling of the lens and by disturbances in the field of view. Various deposits contribute to the soiling of the lens: Hydrometeors (ice, snow, water), dust and dirt are affecting the image quality in variable intensity and duration. Objects in the field of view can be insects or birds that have temporarily settled on the camera. Moreover, it includes objects such as antennas or cranes that may temporarily disturb the image. Although the installed preventive measures at each ASI in Eye2Sky such as ventilation and heating systems or automatic cleaning reduce deposits (see also section 3), detection is an important quality control task. A manual and visual control of multisite daily image acquisition makes use of keograms and image statistics (e.g. long-term mean, outliers, extreme values). Fig. 7 shows examples of typical quality issues and how the detection in keograms and daily mean images support daily QC. Keograms have been introduced to detect aurora borealis (Eather et al. 1976; Lay et al. 2016; English et al. 2024) and have been suggested by Stut et al. (2020) for the summary of cloud development. Moreover, persistent lens soiling can be identified in horizontal stripes, short-lasting events such as insects and birds are obvious as dark spots in the image. While daily mean images smooth out cloud dynamics as well as short-lasting events (e.g. birds, insects), persistent soiling is made visible as deviations from the mean. Automatic detection of single images disturbed by birds, insects or even human faces is currently under development.

Daily mean images are also used to identify the static horizon outline. While the horizon is assumed to be static

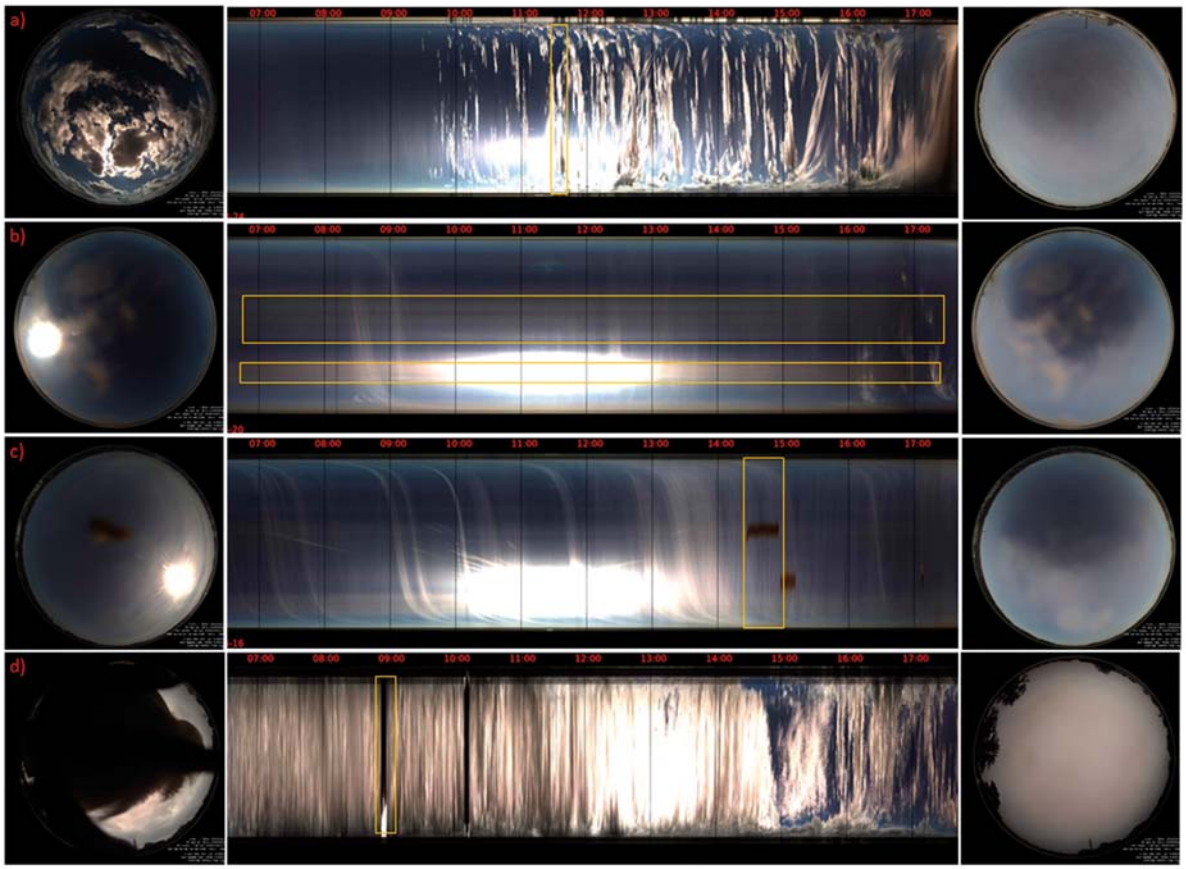

Fig. 7. Examples of different images qualities with raw image (left), daily keogram (center) and daily mean (right) for 4 typical conditions: a) A cleaned ASI at station OLUOL. b) Dust deposit on ASI at station EMSTE after sahara dust event in April 2022 on an almost clear sky day. c) Insects on camera lens of ASI at station PVNOR with few thin cirrus. d) Bird on ASI at station BARSE during cloudy day. Keograms are generated from vertical stripes out of the center of each image per day.

during a day, it can be identified better with edge detection algorithms in long-term averages than in single images.

5.2 Quality control for solar irradiance and meteorological measurements

The quality control (QC) for the solar irradiance and meteorological measurements in Eye2Sky consists of a **manual** and an **automatic** quality control. Fig. 8 visualizes the data processing and data products.

For the manual control, known data errors due to technical issues with instrumentation or due to other known reasons are logged in an internal text file. It includes technical problems which are typically solar tracker failures (no or wrong tracking) or defects of sensors. In addition, maintenance visits affecting the data quality (e.g. replacement of sensors or realignment of sensors) are logged here. This file logs timestamps and the measured parameters affected. In a first step, raw data files are cleaned from these obviously wrong measurements. Data that has been removed in this step is flagged and marked in the next step.

In the next step, an automatic quality control is applied. Here, several tests are performed on minutely averaged data. Each test is represented by an integer value. For example, a failing shading test sets the bit 14 to 1, whereas no shading is indicated by 0. Since for each flag a separate bit is used, the combination of failed tests can be represented with a single decimal value. For the given example, if the shading test (bit 14, decimal 4096) and the closure test (bit 6, decimal 32) have failed, the flag's value is 4096 + 32 = 5028. This combined flag value is added to a new data set representing the QC results for each parameter and time step.

A quality controlled and cleaned data set is achieved with replacing data according to their QC-flags. Since not all QC-flags represent necessarily an erroneous measurement, in the proposed cleaning procedure only certain tests are considered for a removal of data points. For short-lasting cleaning events (bit 12, decimal 1024) an interpolation between subsequent data points is applied. See Table 4 for details on QC tests and their handling in cleaning the data.

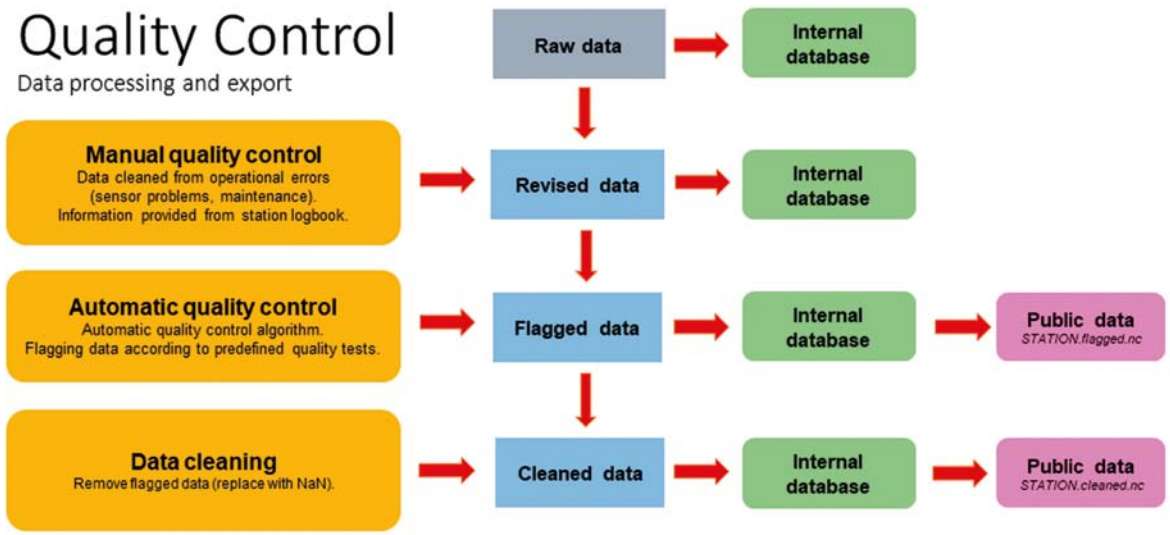

Fig. 8. Overview of the quality control and data export procedure for meteorological data from Eye2Sky.

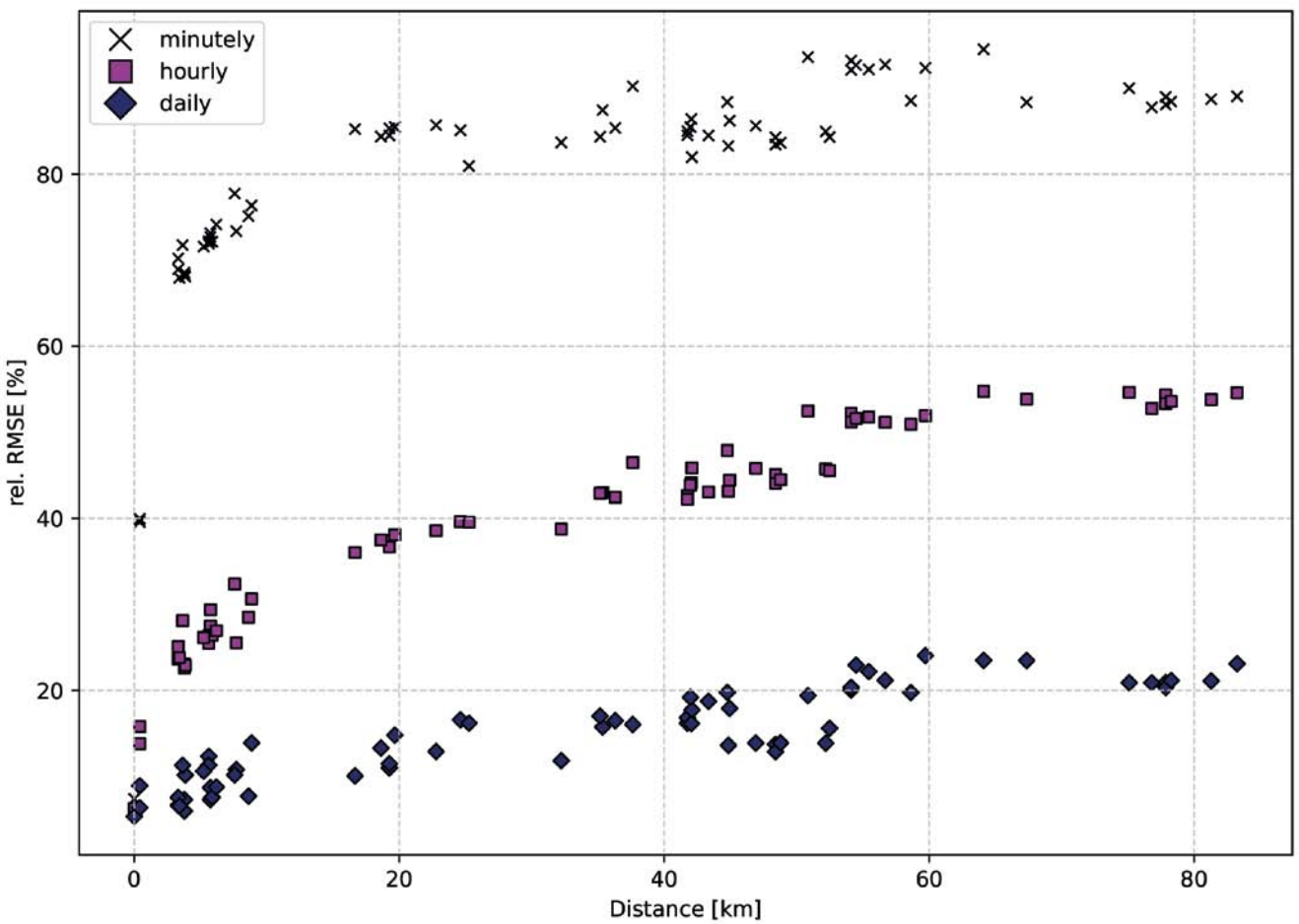

Fig. 9. Variogram of GHI measurements in Eye2Sky for the period April 2022–March 2023. Analogue to Zelenka et al. (1999) the relative root mean square error (RMSE) between any pair of stations in the network is plotted as a function of inter-station distance and for minutely, hourly and daily averages.

Table 4. Summary of tests applied to the sensor measurements. Entries in rows "Revised data" and "Cleaned data" inform on the action taking place on data points flagged by the specific test. An "x" indicates that this test has been applied to the parameter.

	Unit	Missing data	Maximum gradient limit	Minimum gradient limit	Tracker-Off Test	Sensor Redundancy	BSRN Closure's / GTI model comparison	Coherence test 2	Extremely rare limit	Physical limit	PU check	Cleaning	Manual flag	Shading
Bits position		0	1	2	3	4	5	6	7	8	10	11	12	13
Decimal value		1	2	4	8	16	32	64	128	256	512	1024	2048	4096
Revised data		remove	keep	keep	keep	keep	keep	keep	keep	keep	remove	keep	remove	keep
Cleaned data		remove	remove	keep	keep	keep	keep	keep	keep	remove	remove	interpolate	remove	remove
GHI	W m^{-2}	x				x	x	x	x	x	x	x	x	x
DHI	W m^{-2}	x			x	x	x	x	x	x	x	x	x	
DNI	W m^{-2}	x			x	x	x		x	x	x	x	x	x
GTI	W m^{-2}	x					x			x		x	x	x
Wind speed	m s^{-2}	x	x	x						x			x	
Wind direction	°	x								x			x	
Air temperature	°C	x	x	x						x			x	
relative Humidity	%	x	x	x						x			x	
Precipitation	mm		x											
Barometric pressure	hPa		x											

We provide both *flagged* and *cleaned* data files. While advanced users might work with the former and either apply their own QC or decide on a different handling of flagged data, applied users may directly use the *cleaned* version. Fig. 10 shows the Visual QC performed by the *libinsitu* (Blanc et al. 2022) for the reference station OLWIN and the RSI-based station OLDON.

For all automatic QC tests, auxiliary data used for quality control are the position of the sun (Spencer 1972) and the irradiance in clear sky situations (Rigollier et al. 2000) using a climatology of turbidity as input (Remund & Domeisen 2009). One must be aware, that different models for sun position and clear sky irradiance will affect the QC results to some extent. In the following the individual QC tests are described.

5.2.1 Missing data

Missing values are often the result of sensor failures, the failure of the entire station or long-term connectivity problems.

5.2.2 Maximum and minimum gradient limits

This test is useful to detect unrealistic change rates or stagnation in measurements. The limits used are presented in Table 5 and based on previous work from Espinar et al. (2012) and Geuder et al. (2015). Measurements failing exceeding the allowed maximum gradient limits are removed for the cleaned version of the data set.

5.2.3 Tracker-off test

The tracker-off test formulated by Long & Shi (2008) is a test for the proper tracking of the sun tracker by testing if the tracker is shading the diffuse irradiance sensor correctly. It tests the diffuse fraction (fraction of diffuse (ratio of diffuse to global irradiance) under sunny conditions, which is defined as a clear sky index (ratio of global to clear sky global irradiance) > 0.85. It gives a failure if the diffuse fraction exceeds a threshold value of 0.85.

5.2.4 Sensor redundancy test

For RSI-based solar irradiance measurements, two photodiodes are used. For further data processing only measurements from one sensor are taken, which is by definition the northern sensor. Measurements from the second sensor can be used for redundancy and to test if the readings are reliable. Here, only large deviations between both readings are focused to detect short-term or systematic problems with one of the sensors. GHI, DHI and DNI measurements are flagged if both sensors differ more than 10% (GHI, DNI) and 20% (DHI) divided by their corresponding clear sky values:

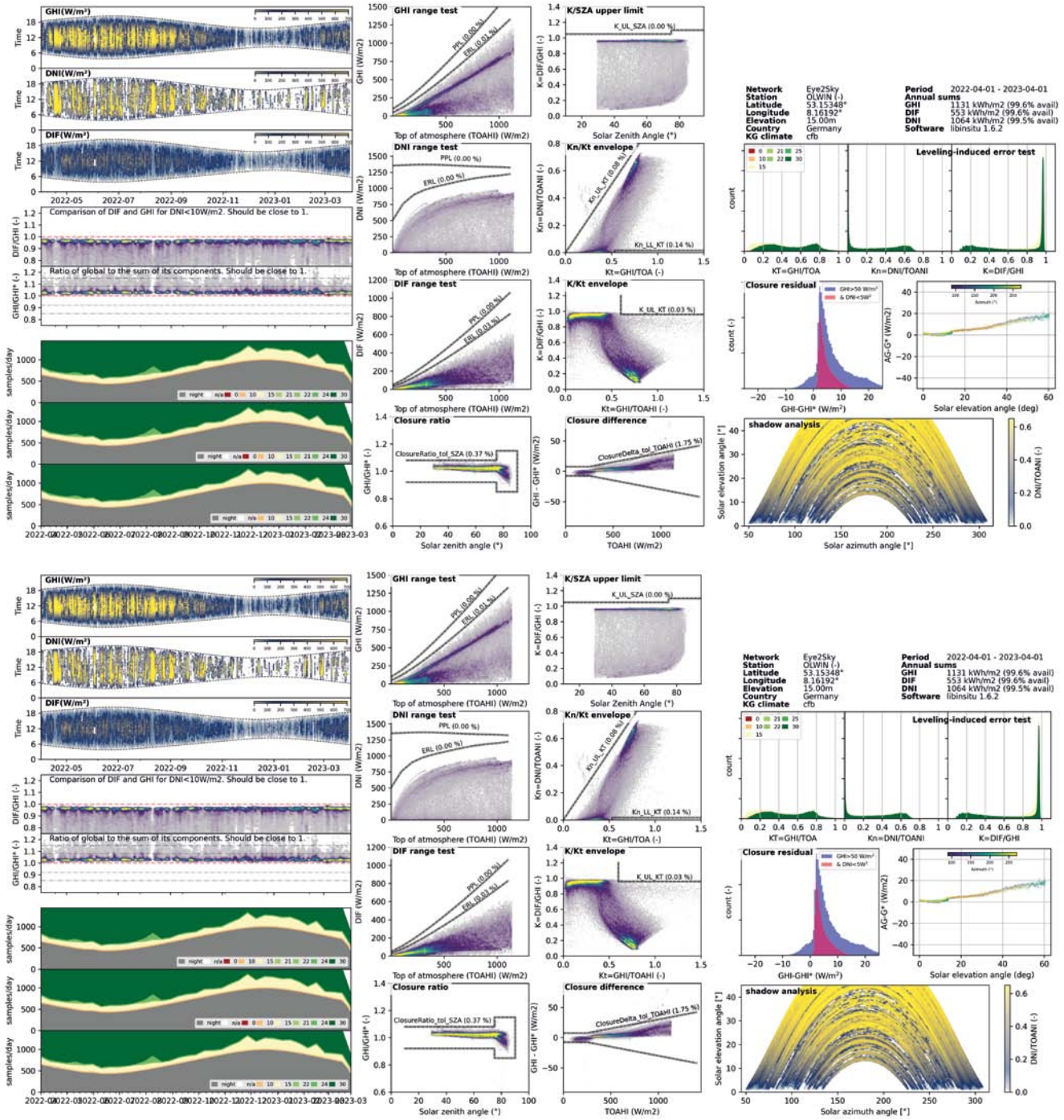

Fig. 10. Visual Quality Check from *libinsitu* applied to OLWIN (top) and OLDON (bottom) data from 1 April 2022 to 1 April 2023.

Table 5. Limits used in the minimum and maximum gradient tests. Values taken from (Espinar et al. 2012) and (Geuder et al. 2015).

Parameter	Min Gradient	Max Gradient
Wind speed	0.5 [m/s/h]	20 [m/s/2min]
Air temperature	0.1 [K/h]	3 [K/min]
Relative humidity	0.1 [%/2h]	10 [%/min]
Precipitation	-	4 [mm/min]
Barometric pressure	-	2 [hPa/min]

Table 6. Values used for the physical limit tests. GHI_{max}, DHI_{max}, DNI_{max}, GTI_{max} are computed based on formulas from Long & Shi (2008); Long & Dutton (2010) and Lorenz et al. (2022).

Parameter	Lower physical limit	Upper physical limit
GHI	-4W m^{-2}	GHI_{max}
DHI	-4W m^{-2}	DHI_{max}
DNI	-4W m^{-2}	DNI_{max}
GTI	GTI_{min}	GTI_{max}
Wind speed [m s^{-1}]	0.3	100
Wind direction [°]	0	360
Relative humidity [°C]	5	100
Air temperature [°C]	-40	60
Precipitation [mm/10min]	0	100

$$\frac{|DHI_1 - DHI_2|}{DHI_{clear}} < 0.2 \; \frac{|DNI_1 - DNI_2|}{DNI_{clear}} < 0.1 \frac{|GHI_1 - GHI_2|}{GHI_{clear}} < 0.1 \qquad (5.1)$$

5.2.5 BSRN's closure equation test

When the three components of irradiance are measured independently, GHI, DHI and DNI is coherent and the sum of measured DHI and direct horizontal irradiance must be close to the value of measured GHI. For this test, formulae and thresholds defined by (Long & Shi 2008) and (Long & Dutton 2010) are used.

5.2.6 Consistency test for global tilted irradiance

For global tilted irradiance (GTI) measurements in Eye2Sky, a QC proposed by Lorenz et al. (2022) is used. Here, the measured GTI is compared to a modelled global tilted irradiance GTI_{mod} using a transposition model with GHI and DHI measurements as input. Different to the original version of Lorenz et al. (2022), a lower threshold of 100 Wm^{-2} is used. Data points are flagged, if

$$|GTI_{mod} - GTI| > 100\,\mathrm{W}\,m^{-2}. \qquad (5.2)$$

To compute GTI_{mod} the updated Perez diffuse sky model from Driesse et al. (2024) is applied providing GHI, DHI and DNI measurements. For stations not providing a DHI measurement (PVAMM, OLJET), a diffuse fraction model (Driesse et al. 2024) estimates DHI and DNI from measured GHI. For both calculations the implementations in the Python library PVlib (Anderson et al. 2023) are used.

5.2.7 Coherence between GHI and DHI

This test is applied to check if the independently measured GHI and DHI are within sensible limits of instruments and are coherent. According to this test DHI should not be higher than GHI within the limits of accuracy (Long & Shi (2008); Long & Dutton (2010)).

5.2.8 Extremely rare upper observation limit

This test is applied to solar irradiance parameters only. The extremely rare upper observation limits from the BSRN Global Network recommended QC tests by Long & Shi (2008); Long & Dutton (2010) are used. When a value exceeds the rare limit, the observation should be analyzed manually. It does not automatically indicate an erroneous measurement.

5.2.9 Physically possible limits

This test is applied to all parameters. The physical limits from the BSRN (baseline surface radiation network) recommended QC tests by Long & Shi (2008); Long & Dutton (2010) are used for GHI, DNI and DHI and the defined limits for auxiliary meteorological parameters are set to identify non-plausible outliers and can be adapted in different climates. The physical limits for GTI are defined by Lorenz et al. (2022). The upper physical limits for solar irradiance values are dynamic values depending on solar zenith angle for each timestamp. Table 6 presents the used physical limits. Measurements that exceed the limits are removed in the cleaned data set.

5.2.10 PU check

This test is only applied to RSI sensors and checks the raw data from each pyranometer unit (PU). The test fails if the raw signal falls below a threshold of −50 Wm^{-2} and indicates unreliable measurements. As the test is only applied to raw data, these are already removed for the revised raw data set.

5.2.11 Cleaning

Our data loggers are equipped with a so-called "maintenance" button. Once pressed, time stamps are marked in raw data files. Cleaning of sensors affect measurements for a few seconds. In our data quality control procedure, GHI, DHI and DNI measurements are flagged when a maintenance event has happened. For quality-controlled data, these data points are removed and measurements from the timestamp before and after the event used for gap-filling by interpolation.

5.2.12 Manual flag

Data quality issues due to technical problems with the instrumentation or data loggers as well as human-induced measurement errors (e.g. during maintenance) are logged in an internal logbook. The entries are used to flag the affected readings. Because this kind of erroneous data cannot be detected reliably by automatic quality control procedures, a revised version of our raw data files with these data points removed is stored separately in our data base.

5.2.13 Shading

Shading caused by objects in the horizon of the solar radiation measurement instrument affects direct irradiance and to a smaller extent global irradiance. The impact on diffuse radiation is rather small. Data points affected by shading are therefore flagged during the QC process. Shading due to the orographic structures of a site's horizon can be computed based on digital elevation models and are often implemented in publicly available tools (e.g. PVGIS https://re.jrc.ec.europa.eu/pvg_tools/en/). On the other hand, shading by nearby objects such as buildings, towers, antennas or even cable lines can hardly be computed without the knowledge of nearby objects and their positioning with respect to the instrumentation. A data-driven approach for detecting all kind of shading is the analysis of long-term timeseries (at least one year) of solar radiation measurements with respect to the sun's elevation and azimuth angle summarized in a single graph, a so called *horse shoe plot*. Here, the impact of shading on direct irradiance and to a lesser extent on global irradiance is emphasized visually. Fig. 11 shows such a graph for yearly data from station PVNOR. While other studies used machine learning approaches (Lorenz et al. 2022), this has been conducted manually for Eye2Sky. The result is a horizon profile for all solar azimuth angles. DNI, GHI or GTI measurements are flagged as shaded, when the corresponding sun position (elevation angle) is below this horizon line. These measurements are removed for the cleaned data set. For objects that do not touch the ground, a lower horizon marks the lower position of this object (see blue line in Fig. 11).

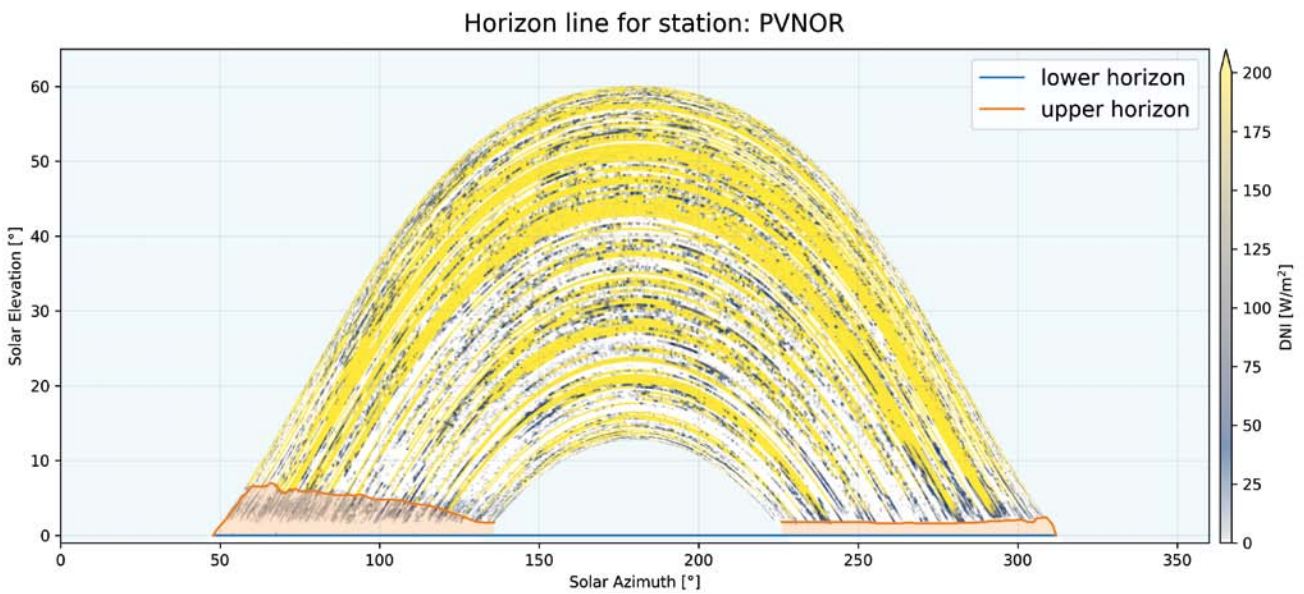

Fig. 11. Shading analysis for station PVNOR for one year of DNI measurements. The detected horizon is shaded in red.

6 Applications

The main objective of the Eye2Sky network is the development and application of nowcasting methods for the short-term prediction of solar radiation in the context of solar energy systems. While the method development focuses on the optimal processing and merging of various located ASI (Blum et al. 2021, 2022; Blum 2022) and the combination with satellite images (Lezaca Galeano et al. 2022, 2024), the integration of the methods output in existing and virtual applications is a second focus of Eye2Sky.

Blum et al. highlight the benefit of nowcasts from a ASI network compared to ASI pairs and persistence with a root mean square deviation (RMSD) of 136 Wm^{-2} compared to 173 Wm^{-2} and 213 Wm^{-2}, respectively (Blum et al. 2022; Blum 2022). Moreover, further improvements could be yield by blending nowcast data from multiple sources with linear regression. Lezaca Galeano et al. (2024) showed that an error reduction of 3.5% to 9% compared to the raw predictions from the ASI network and satellite data is possible.

The use of an ASI network for the prediction of PV power production for either decentralized single rooftop systems or larger standalone PV plants has been studied by Blum (2022), Schaible et al. (2024) and Scheper (2025). Scheper (2025) investigated the impact of different network designs with a reduced number of ASI in the Eye2Sky network on nowcasting results for two different virtual use cases. First, all suitable roofs in the city of Oldenburg (local solar roof cadastre) have been equipped with PV installations accumulating in 100, 479 roofs and 892 MW. Second, a virtual large scale PV plant located in the center of the network with 250MW installed capacity has been assumed. The thesis could show, that an optimized network with a reduced number of ASI to save installation and maintenance costs can guarantee high nowcasting quality compared to the full Eye2Sky network in the vicinity of the use cases. On the other hand, ASI networks installed in large scale PV plants benefit of additional ASI in the surroundings, especially for longer forecast horizons.

It is important to note, that depending on the applications' need, forecasting strategies are optimized for the objective of the application. Schaible et al. (2024) studied the use of ramp-forecasting for PV plants equipped with battery storage to smooth short-term power output fluctuations. The authors found, that although ASI-based nowcasts cannot completely replace batteries, they substantially reduce the need for such storage solutions.

Furthermore, the availability of spatial and temporal high resolution solar radiation information allows also for in-depth scientific research on the characteristics of solar resources at a scale resolving even the smallest fraction of clouds. Schmidt et al. (2023b) showed that solar irradiance products based on Eye2Sky data have significant higher level of detail than products based on satellite images or numerical weather models in presence of small-scale clouds. This is currently used to assess the latest generation of high resolution climate models as provided in the Destination Earth program or to assess mesoscale modeling as provided e.g. the ICON-D2 model.

7 Public data set

Eye2Sky data has been made partially publicly available. The data is hosted on Zenodo https://zenodo.org/records/12804613 (Schmidt et al. 2024). The data should allow the scientific community to use the unique data set acquired in the past years of operating the Eye2Sky network. We aim to provide a data set that supports in training and testing models. Therefore one full year (April 2022–March 2023) of meteorological and ceilometer data as well as 4 month of ASI images (April 2022–July 2022) from all stations is published. From the reference station (OLWIN/OLUOL) ASI images are provided for the full year. All images make up approximately 1.6 Terabytes of data.

Measurement data is provided in two versions: A version with raw data and additional flags for quality control results and a version with cleaned data, that is ready to use for most applications. The files also include additional clear sky model data of GHI, DHI, DNI and sun position information used for quality control.

Image masks and calibration data for processing of images are provided as well. Please refer to this article and the data set DOI when using the data in your research.

The data set thus complements the list of open data ASI images (Nie et al. 2024) and solar irradiance measurements (https://viewer.webservice-energy.org/in-situ/).

8 Conclusion

In this publication the Eye2Sky measurement network has been described regarding its design, data acquisition and data control procedures. Furthermore, the received measurement and image data sets and the results from first studies based on Eye2Sky's data have been presented.

The operational Eye2Sky network in north-western Germany can be seen as the first infrastructure of its kind. It consists of 29 all-sky imagers (ASI) and 11 meteorological and solar irradiance measurements within an area of 110 km × 100 km. With its dedicated design, the Eye2Sky network offers a large potential for the development of novel very short-term forecasting methods for the integration of PV power into electrical grids.

Since 2018, the network has been continuously collecting sky images and measurements of direct, diffuse and global irradiance. Eye2Sky already delivered a large database of ASI images and solar irradiance measurements. Extensive quality control procedures consisting of manual and automatic methods have been implemented to guarantee high

quality data sets. The impact of using automatic cleaning systems and irregular event detection tools is currently investigated to prepare a next evolution of the network. This also includes the definition of operational procedures to identify maintenance needs at remote measurement stations.

With this publication a data set of measurements from 11 stations for the 1-year period from April 2022 to March 2023 and ASI images from 29 ASIs for the 4-month period from April to July 2022 has been published. ASI images from the reference station (OLWIN/OLUOL) are provided additionally for the full year. Provision of additional ASI data can be discussed on request.

The solar irradiance data sets are provided with quality control information and in common scientific data format. Raw camera images come with additional calibration details to help researchers using the data for their developments and investigations.

The unique data set presented in this publication will be valuable for a multitude of local and high resolution nowcasting approaches and scientific research. Several studies based on Eye2Sky and other infrastructures already revealed that the usage of multiple cameras in a network reduce forecast uncertainties compared to methods based on single or pairs of cameras. Multi-source approaches utilising the advantages of each data input (e.g. ground-based measurements, ASI and satellite-based nowcasts, large eddy simulation, numerical weather prediction) will lead to a new generation of more accurate and seamless forecasting technologies for the very short-term horizon of 0–360 min ahead. The authors are currently engaged in an intensive exchange with stakeholders such as plant operators, grid operators and energy traders. Feedback from stakeholders on needs and requirements will support us to adapt nowcasting strategies to specific applications.

Acknowledgements: The establishment and operation of the Eye2Sky network was only possible with the help of many people. We therefore thank all institutions and companies who offered hosting a station and all colleagues who contributed with technical, administrative and legal support.

References

Aides, A., Levis, A., Holodovsky, V., Schechner, Y. Y., Althausen, D., &Vainiger, A. (2020). Distributed sky imaging radiometry and tomography. In: *2020 IEEE International Conference on Computational Photography (ICCP),* 1–12 https://doi.org/10.1109/ICCP48838.2020.9105241

Anderson, K. S., Hansen, C. W., Holmgren, W. F., Jensen, A. R., Mikofski, M. A., &Driesse, A. (2023). pvlib python: 2023 project update. *Journal of Open Source Software, 8*(92), 5994. https://doi.org/10.21105/joss.05994

Antonanzas, J., Osorio, N., Escobar, R., Urraca, R., Martinez-de-Pison, F. J., &Antonanzas-Torres, F. (2016). Review of photovoltaic power forecasting. *Solar Energy, 136*, 78–111. https://doi.org/10.1016/j.solener.2016.06.069

Blanc, P., Jolivet, R., Ménard, L., &Saint-Drenan, Y. M. (2022). Data sharing of in-situ measurements following GEO and FAIR principles in the solar energy sector. https://doi.org/10.23646/AC2M-8504

Blum, N. (2022). Nowcasting of solar irradiance and photovoltaic production using a network of all-sky imagers. Ph.D. thesis, RWTH Aachen. https://publications.rwth-aachen.de/record/957472

Blum, N. B., Nouri, B., Wilbert, S., Schmidt, T., Lünsdorf, O., Stührenberg, J., … Pitz-Paal, R. (2021). Cloud height measurement by a network of all-sky imagers. *Atmospheric Measurement Techniques, 14*(7), 5199–5224. https://doi.org/10.5194/amt-14-5199-2021

Blum, N. B., Wilbert, S., Nouri, B., Stührenberg, J., Lezaca Galeano, J. E., Schmidt, T., … Pitz-Paal, R. (2022). Analyzing spatial variations of cloud attenuation by a network of all-sky imagers. *Remote Sensing, 14*(22), 5685. https://doi.org/10.3390/rs14225685

Chu, Y., Li, M., Pedro, H. T., &Coimbra, C. F. (2022). A network of sky imagers for spatial solar irradiance assessment. *Renewable Energy, 187*, 1009–1019. https://doi.org/10.1016/j.renene.2022.01.032

Craciun, B. I., Kerekes, T., Séra, D., Teodorescu, R., &Annakkage, U. D. (2017). Power ramp limitation capabilities of large pv power plants with active power reserves. *IEEE Transactions on Sustainable Energy, 8*(2), 573–581. https://doi.org/10.1109/TSTE.2016.2612121

Driesse, A., Jensen, A. R., &Perez, R. (2024). A continuous form of the perez diffuse sky model for forward and reverse transposition. *Solar Energy, 267*, 112093. https://doi.org/10.1016/j.solener.2023.112093

Eather, R. H., Mende, S. B., &Judge, R. J. R. (1976). Plasma injection at synchronous orbit and spatial and temporal auroral morphology. *Journal of Geophysical Research, 81*(16), 2805–2824. https://doi.org/10.1029/JA081i016p02805.

English, A., Stuart, D. J., Hampton, D. L., &Datta-Barua, S. (2024). Automated nighttime cloud detection using keograms when aurora is present. *Earth and Space Science, 11*(1), e2022EA002808. https://doi.org/10.1029/2022EA002808

Espinar, B., Blanc, P., Wald, L., Hoyer-Klick, C., Schroedter Homscheidt, M., &Wanderer, T. (2012). On quality control procedures for solar radiation and meteorological measures, from subhourly to montly average time periods. *EGU General Assembly 2012*. https://minesparis-psl.hal.science/hal-00691350.

Fabel, Y., Nouri, B., Wilbert, S., Blum, N., Triebel, R., Hasenbalg, M., … Pitz-Paal, R. (2022). Applying self-supervised learning for semantic cloud segmentation of all-sky images. *Atmospheric Measurement Techniques, 15*(3), 797–809. https://doi.org/10.5194/amt-15-797-2022

Fabel, Y., Nouri, B., Wilbert, S., Blum, N., Schnaus, D., Triebel, R., … Pitz-Paal, R. (2024). Combining deep learning and physical models: A benchmark study on all-sky imager-based solar nowcasting systems. *Solar RRL, 8*(4), 2300808. https://doi.org/10.1002/solr.202300808

Geuder, N., Affolter, R., Eckl, M., Kraas, B., & Wilbert, S. (2012). Measurement accuracy of twin-sensor rotating shadowband irradiometers (rsi). *SolarPACES 2012*. https://elib.dlr.de/78578/

Geuder, N., Wolfertstetter, F., Wilbert, S., Schüler, D., Affolter, R., Kraas, B., … Espinar, B. (2015). Screening and flagging of solar irradiation and ancillary meteorological data. *Energy Procedia, 69*, 1989–1998. https://doi.org/10.1016/j.egypro.2015.03.205

Ghosh, S., Rahman, S., &Pipattanasomporn, M. (2017). Distribution voltage regulation through active power curtailment with pv inverters and solar generation forecasts. *IEEE Transactions on Sustainable Energy, 8*(1), 13–22. https://doi.org/10.1109/tste.2016.2577559

Howie, R. M., Paxman, J., Bland, P. A., Towner, M. C., Cupak, M., Sansom, E. K., &Devillepoix, H. A. R. (2017). How to build a continental scale fireball camera network. *Experimental Astronomy, 43*(3), 237–266. https://doi.org/10.1007/s10686-017-9532-7

Kaur, A., Nonnenmacher, L., Pedro, H. T., &Coimbra, C. F. (2016). Benefits of solar forecasting for energy imbalance markets. *Renewable Energy, 86*, 819–830. https://doi.org/10.1016/j.renene.2015.09.011

Lave, M., Kleissl, J., &Arias-Castro, E. (2012). High-frequency irradiance fluctuations and geographic smoothing. *Solar Energy, 86*(8), 2190–2199. https://doi.org/10.1016/j.solener.2011.06.031

Lay, S., Vermeulen, J., Perin, C., Donovan, E., Dachselt, R., & Carpendale, S. (2016). Slicing the aurora: An immersive proxemics-aware visualization. *Proceedings of the 2016 ACM Companion on Interactive Surfaces and Spaces,* 91–97. https://doi.org/10.1145/3009939.3009954

Lezaca Galeano, J. E., Hammer, A., Lünsdorf, O., Schmidt, T., & Blum, N. (2022). High resolution hybrid forecast based on the combination of satellite and an all sky imager network forecasts. EMS Annual Meeting 2022. https://elib.dlr.de/190483/

Lezaca Galeano, J. E., Hammer, A., Schmidt, T., & Stührenberg, J. (2024). The benefit of a dense network of all-sky imagers for regional satellite-based short-term forecasts of solar irradiance. PV-Symposium. https://elib.dlr.de/211273/

Logothetis, S. A., Salamalikis, V., Wilbert, S., Remund, J., Zarzalejo, L. F., Xie, Y., … Kazantzidis, A. (2022). Benchmarking of solar irradiance nowcast performance derived from all-sky imagers. *Renewable Energy, 199*, 246–261. https://doi.org/10.1016/j.renene.2022.08.127

Lohmann, G. (2018). Irradiance variability quantification and small-scale averaging in space and time: A short review. *Atmosphere, 9*(7), 264. https://doi.org/10.3390/atmos9070264

Long, C. N., E. G. Dutton, 2010:BSRN global network recommended QC tests v2.0. https://epic.awi.de/id/eprint/30083/1/BSRN_recommended_QC_tests_V2.pdf

Long, C. N., &Shi, Y. (2008). An automated quality assessment and control algorithm for surface radiation measurements. *The Open Atmospheric Science Journal, 2*(1), 23–37. https://doi.org/10.2174/1874282300802010023

Lorenz, E., Guthke, P., Dittmann, A., Holland, N., Herzberg, W., Karalus, S., … Saint-Drenan, Y. M. (2022). High resolution measurement network of global horizontal and tilted solar irradiance in southern germany with a new quality control scheme. *Solar Energy, 231*, 593–606. https://doi.org/10.1016/j.solener.2021.11.023

Ma Lu, S., Zainali, S., Stridh, B., Avelin, A., Amaducci, S., Colauzzi, M., &Campana, P. (2022). Photosynthetically active radiation decomposition models for agrivoltaic systems applications. *Solar Energy, 244*, 536–549. https://doi.org/10.1016/j.solener.2022.05.046

Macke, A., Seifert, P., Baars, H., Barthlott, C., Beekmans, C., Behrendt, A., … Xie, X. (2017). The HD(CP)²observational prototype experiment (HOPE) – an overview. *Atmospheric Chemistry and Physics, 17*(7), 4887–4914. https://doi.org/10.5194/acp-17-4887-2017

Mahdavi, N., Braslavsky, J. H., Seron, M. M., &West, S. R. (2017). Model predictive control of distributed airconditioning loads to compensate fluctuations in solar power. *IEEE Transactions on Smart Grid, 8*(6), 3055–3065. https://doi.org/10.1109/tsg.2017.2717447

Meddahi, A., Tuomiranta, A., &Guillon, S. (2025). Skill-driven data sampling and deep learning framework for minute-scale solar forecasting with sky images. *Solar RRL, 9*(4), 2400664. https://doi.org/10.1002/solr.202400664

Mejia, F. A., Kurtz, B., Levis, A., de la Parra, Í., &Kleissl, J. (2018). Cloud tomography applied to sky images: A virtual testbed. *Solar Energy, 176*, 287–300. https://doi.org/10.1016/j.solener.2018.10.023

Nie, Y., Li, X., Paletta, Q., Aragon, M., Scott, A., &Brandt, A. (2024). Open-source sky image datasets for solar forecasting with deep learning: A comprehensive survey. *Renewable & Sustainable Energy Reviews, 189*, 113977. https://doi.org/10.1016/j.rser.2023.113977

Notton, G., Nivet, M. L., Voyant, C., Paoli, C., Darras, C., Motte, F., &Fouilloy, A. (2018). Intermittent and stochastic character of renewable energy sources: Consequences, cost of intermittence and benefit of forecasting. *Renewable & Sustainable Energy Reviews, 87*, 96–105. https://doi.org/10.1016/j.rser.2018.02.007

Nouri, B., Kuhn, P., Wilbert, S., Prahl, C., Pitz-Paal, R., Blanc, P., … Heineman, D., 2018:Nowcasting of dni maps for the solar field based on voxel carving and individual 3d cloud objects from all sky images. *AIP Conference Proceedings, 2033*(1), 190011. https://doi.org/10.1063/1.5067196

Nouri, B., Kuhn, P., Wilbert, S., Hanrieder, N., Prahl, C., Zarzalejo, L., … Pitz-Paal, R. (2019a). Cloud height and tracking accuracy of three all sky imager systems for individual clouds. *Solar Energy, 177*, 213–228. https://doi.org/10.1016/j.solener.2018.10.079

Nouri, B., Wilbert, S., Segura, L., Kuhn, P. M., Hanrieder, N., Kazantzidis, A., … Pitz-Paal, R. (2019b). Determination of cloud transmittance for all sky imager based solar nowcasting. *Solar Energy, 181*, 251–263. https://doi.org/10.1016/j.solener.2019.02.004

Nouri, B., Blum, N., Wilbert, S., &Zarzalejo, L. F. (2022). A hybrid solar irradiance nowcasting approach: Combining all sky imager systems and persistence irradiance models for increased accuracy. *Solar RRL, 6*(5), 2100442. https://doi.org/10.1002/solr.202100442

Paletta, Q., Arbod, G., &Lasenby, J. (2021). Benchmarking of deep learning irradiance forecasting models from sky images an in-depth analysis. *Solar Energy, 224*, 855–867. https://doi.org/10.1016/j.solener.2021.05.056

Peng, Z., Yu, D., Huang, D., Heiser, J., Yoo, S., &Kalb, P. (2015). 3d cloud detection and tracking system for solar forecast using multiple sky imagers. *Solar Energy, 118*, 496–519. https://doi.org/10.1016/j.solener.2015.05.037

Perez, R. (2018). *Wind Field and Solar Radiation Characterization and Forecasting: A Numerical Approach for Complex Terrain Green Energy and Technology Ser*. Cham:Springer. https://doi.org/10.1007/978-3-319-76876-2

Ranalli, J., Peerlings, E. E., & Schmidt, T. (2020). Cloud advection and spatial variability of solar irradiance. 47th IEEE Photovoltaic Specialists Conference (PVSC), 37–44. https://doi.org/10.1109/PVSC45281.2020.9300700

Remund, J., & Domeisen, D. (2009). Aerosol optical depth and Linke turbidity climatology. IEA SHC Task, 36. https://meteonorm. com/assets/publications/ieashc36_report_TL_AOD_climatologies.pdf

Rigollier, C., Bauer, O., &Wald, L. (2000). On the clear sky model of the esra european solar radiation atlas with respect to the heliosat method. *Solar Energy, 68*(1), 33–48. https://doi.org/10.1016/S0038-092X(99)00055-9

Ryu, A., Ishii, H., &Hayashi, Y. (2021). Battery smoothing control for photovoltaic system using short-term forecast with total sky images. *Electric Power Systems Research, 190*, 106645. https://doi.org/10.1016/j.epsr.2020.106645

Saleh, M., Meek, L., Masoum, M. A. S., &Abshar, M. (2018). Battery-less short-term smoothing of photovoltaic generation using sky camera. *IEEE Transactions on Industrial Informatics, 14*(2), 403–414. https://doi.org/10.1109/tii.2017.2767038

Scaramuzza, D., Martinelli, A., & Siegwart, R. (2006). A toolbox for easily calibrating omnidirectional cameras. *International Conference on Intelligent Robots and Systems*. https://doi.org/10.1109/iros.2006.282372

Schaible, J., Nouri, B., Höpken, L., Kotzab, T., Loevenich, M., Blum, N., … Wilbert, S. (2024). Application of nowcasting to reduce the impact of irradiance ramps on pv power plants. *EPJ Photovoltaics, 15*, 15. https://doi.org/10.1051/epjpv/2024009

Scheper, A. (2025). On the design of eye2sky camera network subsets for the optimal nowcast of pv production. Master's thesis, Carl von Ossietzky Universität Oldenburg https://elib.dlr.de/211689/

Schmidt, T. (2017). High resolution solar irradiance forecasts based on sky images. Ph.D. thesis, University Oldenburg https://oops.uni-oldenburg.de/id/eprint/3232

Schmidt, T., Kalisch, J., Lorenz, E., &Heinemann, D. (2016). Evaluating the spatio-temporal performance of sky-imager-based solar irradiance analysis and forecasts. *Atmospheric Chemistry and Physics, 16*(5), 3399–3412. https://doi.org/10.5194/acp-16-3399-2016

Schmidt, T., Calais, M., Roy, E., Burton, A., Heinemann, D., Kilper, T., &Carter, C. (2017). Short-term solar forecasting based on sky images to enable higher pv generation in remote electricity networks. *Renewable Energy and Environmental Sustainability, 2*, 23. https://doi.org/10.1051/rees/2017028

Schmidt, T., Stührenberg, J., Blum, N., Lezaca Galeano, J. E., Hammer, A., Schroedter-Homscheidt, M., & Vogt, T. (2023a). Comparison of short-term (hour-ahead) solar irradiance forecasts from all-sky imagers and satellite images. International Conference of Energy Meteorology ICEM. https://elib.dlr.de/197562/

Schmidt, T., Stührenberg, J., Schellhorn, M., Blum, N., Lezaca Galeano, J. E., Hammer, A., … Schroedter-Homscheidt, M. (2023b). Solar irradiance nowcasting based on a network of all sky imagers: the value of high-resolution data on variability information. EMS Annual Meeting 2023. https://elib.dlr.de/197508/

Schmidt, T., Stührenberg, J., Blum, N., Lezaca, J., Hammer, A., Wilbert, S., … Vogt, T. (2024). Eye2sky dataset all-sky images and meteorological measurements. https://doi.org/10.5281/zenodo.12804613

Spencer, J. (1972). *Computer estimation of direct solar radiation on clear days*. United States:Sol. Energy;https://doi.org/10.1016/0038-092X(72)90011-4

Spurny, P. (1997). Photographic monitoring of fireballs in Central Europe. In: F. A. Allahdadi, E. K. Casani, T. D. Maclay, F. A. Allahdadi, & T. D. Maclay (eds.), *Small Spacecraft, Space Environments, and Instrumentation Technologies, 3116*, 144–155. International Society for Optics and Photonics. https://doi.org/10.1117/12.293337

Stut, N., Boschert, A., Kaiser, F., Zehner, M., Mayer, B., Mayer, O. (2020). Analyse von Einstrahlungsvolatilität und -überhöhungen in hochaufgelösten Datensätzen des DWD und MIM zur Untersuchung von Korrelationen zu meteorologischen Messdaten. https://www.pv-symposium.de/fileadmin/data/PVSYM/Webinare/Freigegebene_Folien_Stut_geschuetzt.pdf

Xie, W., Liu, D., Yang, M., Chen, S., Wang, B., Wang, Z., … Zhang, C. (2020). Segcloud: A novel cloud image segmentation model using a deep convolutional neural network for ground-based all-sky-view camera observation. *Atmospheric Measurement Techniques, 13*(4), 1953–1961. https://doi.org/10.5194/amt-13-1953-2020

Zelenka, A., Perez, R., Seals, R., &Renné, D. (1999). Effective accuracy of satellite-derived hourly irradiances. *Theoretical and Applied Climatology, 62*(3–4), 199–207. https://doi.org/10.1007/s007040050084

Manuscript received: July 9, 2024
Revisions requested: December 6, 2024
Revised version received: February 1, 2025
Manuscript accepted: February 12, 2025